This is a non peer-reviewed preprint submitted to the Journal of Hydrology:

Analysis of nationwide groundwater monitoring networks using lumped-parameter models

Raoul A. Collenteur[a,b,*], Christian Moeck[a,c], Mario Schirmer[a,d], Steffen Birk[b]

[a]*Institute of Earth Sciences, NAWI Graz Geocenter, University of Graz, Heinrichstrasse 26, Graz, 8010, Austria*
[b]*Eawag, Department Water Resources and Drinking Water (W+T), Ueberlandstr. 133, Duebendorf, CH-8600, Switzerland*
[c]*Swiss Groundwater Network (CH-GNet), Ueberlandstr. 133, Duebendorf, CH-8600, Switzerland*
[d]*University of Neuchatel, Centre of Hydrogeology and Geothermics (CHYN), Rue Emile-Argand 11, Neuchatel, CH-2000, Switzerland*

Abstract

Many countries maintain nationwide groundwater networks to monitor the status of their groundwater resources. For effective groundwater resource management, it is fundamental to understand the groundwater dynamics measured in the individual monitoring wells. Nationwide monitoring networks typically cover multiple aquifer systems with different degrees of environmental complexity. The analysis of the data of such networks thus requires flexible modeling approaches. In this study, we assessed the applicability and performance of lumped-parameter models using impulse response functions, as implemented in the Pastas software, to simulate hydraulic head data from the nationwide groundwater monitoring network in Switzerland. The selected 28 monitoring wells in the network are situated in unconsolidated, relatively shallow aquifers across Switzerland. Given the very diverse topography in the study area, snowmelt processes affect some aquifers, while groundwater-surface water interactions are important in the valleys. Different linear and nonlinear models were tested to take precipitation and potential evaporation

*Raoul.Collenteur@eawag.ch (Corresponding Author)

into account, with a new model developed as part of this study to account for the effect of snow processes on recharge generation. After generally good fits in both the calibration and evaluation were achieved, the models were used to identify and quantify which stresses (e.g., precipitation, river stages) control the groundwater dynamics. The results show that precipitation and evaporation explain large parts of the measured dynamics, and about half of the monitoring wells in the network appear to be influenced by river stages. Explicitly accounting for snow processes in the recharge generating process is found to improve the simulation of the head dynamics across Switzerland, particularly for wells in high-altitude aquifers. This study demonstrates for the first time the applicability of lumped-parameter models using impulse response functions to model heads in Switzerland, and more generally, in climatic settings where snow processes are impacting the head dynamics.

Keywords: Groundwater, Impulse response functions, Pastas, Hydraulic heads,

---

1. Introduction

Groundwater supplies freshwater to human populations and supports groundwater-dependent ecosystems around the world. Because of its importance, groundwater quality and quantity is closely monitored in many countries through nationwide monitoring networks. To assess the current water security as well as help forecast future changes in groundwater availability, it is fundamental to understand and predict the groundwater dynamics observed in the individual monitoring wells (e.g., Taylor et al., 2013). Traditionally, process-based groundwater models are used for this purpose, but at the scale of nationwide networks this may not always be feasible due to constraints in time, financial resources, and data to calibrate such complex models. Bakker and Schaars (2019) argued that, depending on the questions asked, it may be possible to provide answers with much simpler point-scale models. Rather than modeling the groundwater dynamics of (multiple) entire aquifer systems, individual models are created for each measurement well in the monitoring network. Advantages of this approach include lower input data requirements and shorter model development and running times.

In several countries, point-scale models are already used operationally to analyze nationwide monitoring networks and groundwater systems. In the United Kingdom, for example, the British Geological Survey maintains an operational system that uses the lumped-parameter model AquiMod to provide seasonal outlooks of the groundwater levels (Mackay et al., 2014). In the Netherlands, Zaadnoordijk et al. (2019) applied transfer function noise (TFN) models using physically based impulse response functions to analyze tens of thousands of groundwater time series, with precipitation and potential evaporation as stresses driving the groundwater dynamics. The results are shared in an online platform (`https://www.grondwatertools.nl/gwsinbeeld/`) and are continuously improved. Response functions describe the response of the dependent variable (e.g., groundwater levels) to an independent variable (e.g., pumping or recharge). Although Zaadnoordijk et al. (2019) used only precipitation and potential evaporation in the models, a distinct advantage of this type of model is that it is straightforward to add other stresses to the models (von Asmuth et al., 2008). Applications in variety of countries (e.g., India, van Dijk et al. (2019); Brazil, Manzione et al. (2017); the Baltic states, Babre et al. (2022)) have demonstrated that such models are applicable in a variety of climatological and hydrogeological settings, although alternations may be necessary for some locations.

One such alternation, proposed by Peterson and Western (2014), is the inclusion of a root zone model that computes groundwater recharge in the TFN model, and in that way account for the nonlinear head response to precipitation and potential evaporation. In a case study on Australian aquifers, Peterson and Western (2014) showed that this approach improved the simulation of the heads compared to a linear precipitation excess model that is commonly applied to account for the effect of precipitation and evaporation in the model. The use of a nonlinear root zone model was also found to improve the simulation of groundwater levels in Austria (Collenteur et al., 2021). Moreover, Collenteur et al. (2021) showed that the recharge flux estimated with such models compared well to lysimeter data, suggesting that the method may also be suitable to estimate recharge rates. Although the number of studies applying nonlinear models is growing (see, for example, Kong et al., 2021; Shapoori et al., 2015b), applications are still limited to a few geographic locations despite these promising results. More studies are required to further test and demonstrate their general applicability to simulate heads in different hydrogeological and climatological settings.

Particularly with the inclusion of the aforementioned nonlinear root zone models, we argue that TFN models using impulse response functions have become gray-box type models, built on empirical relationships between the stresses and measured groundwater dynamics (see, for example, Liu et al., 2019). Since the terms commonly used to refer to these models, such as 'time series models' or 'transfer-function noise models', have a strong connotation with black-box type of models, we refer to them as 'lumped-parameter models' here. This term is more commonly used in other hydrological disciplines (e.g., rainfall-runoff modeling) to refer to gray-box type models. In this study, lumped-parameter models are applied to model groundwater dynamics, because of their flexibility in model structure and stresses, the ease of model setup, low data requirements, and, foremost, good model performance in calibration and evaluation. Additionally, when adopting the nonlinear approach described earlier it is straightforward to account for additional processes affecting groundwater recharge in the model, such as snowfall and snowmelt.

The objective of this study is to test the applicability of lumped-parameter models and to improve the understanding of groundwater dynamics observed in unconsolidated aquifers in Switzerland. Applications of lumped-parameter models in Switzerland have so far been limited. Groundwater data is, however, commonly available and the Federal Office for the Environment (FOEN) maintains a national groundwater network to monitor the situation and de-

velopment of the groundwater resources in terms of both quality and quantity. The locations of the considered groundwater monitoring wells range from the relatively flat Swiss Plateau to (pre-)alpine settings with high altitudes, and cover various topographical and climatological areas. Given this setting, some aquifers are affected by snow and snowmelt processes. This affects the infiltration pattern and timing, and, through groundwater recharge, the groundwater dynamics and storage (e.g., Meeks et al., 2017). To adapt the models to this new environment, the nonlinear recharge model developed in Collenteur et al. (2021) is extended with a degree-day snow model to take snow processes into account. Specifically, the objectives of this study are as follows:

1. To assess the applicability and performance of different lumped-parameter models to simulate groundwater dynamics for the nationwide groundwater monitoring network in Switzerland.
2. To identify the stresses that can explain the head fluctuations and quantify their relative importance in explaining the measured groundwater dynamics.
3. To assess the impact of the newly implemented snow model routine for model performance, especially for groundwater dynamics in snow impacted regions.

2. Study area and data

2.1. Swiss Groundwater Monitoring Network

In Switzerland, the Federal Office for the Environment (FOEN) operates a national groundwater monitoring network (NAQUA) to provide a representative view of the state and development of groundwater resources in the country. The development of groundwater resources is recorded in terms of both groundwater quality and quantity. In this study, we focus on the analysis of the hydraulic head time series (hereafter 'heads') measured in relatively shallow piezometers in the QUANT module of the network (see Fig. 1a). Of the available 30 piezometers, 28 wells with long-term time series (defined as 15 years of daily head measurements) were selected for further analysis. All selected monitoring wells are located in unconsolidated and unconfined aquifers (see Fig. 1b). These wells are, to the best of our knowledge, not affected by water abstractions and thus groundwater dynamics are driven by groundwater-surface water interaction, snow melt processes and vertical

ID	index	Start	DTW	DTR	Alt.	Prec.	Evap.	Temp.	Snow
1	Buechberg	1993	32	1493	450	879	585	10	19
2	Crêtelongue	1976	1	127	506	623	615	11	9
3	Davos	1978	2	24	1703	1046	372	2	94
4	Ermensee	1989	18	586	476	1120	574	10	18
5	Gossau	1984	7	165	645	1321	552	9	30
6	Hasle	1990	4	170	567	1181	547	9	26
7	Kestenholz	1987	19	11	447	1097	565	9	23
8	Lamone	1981	5	245	311	1703	636	12	4
9	Maienfeld	1975	4	474	506	1063	601	10	17
10	Marthalen	1983	19	521	367	905	591	10	19
11	Massongex	1994	3	416	396	1007	601	11	10
12	Niederbipp	1977	27	406	455	1107	567	9	22
13	Oberglatt	1990	24	614	426	991	583	10	18
14	Oberwichtrach	1990	2	662	532	1080	567	9	23
15	Poschiavo	1990	1	141	969	1002	525	8	18
16	Samedan B	1980	4	612	1709	693	383	2	75
17	Schaffhausen	1987	42	1383	433	904	588	10	19
18	Sennwald	1990	2	253	435	1219	606	11	17
19	Soral	1977	78	1120	448	960	609	11	8
20	Trub	2005	8	54	791	1484	498	7	47
21	Utzenstorf	1990	7	159	483	1064	565	9	21
22	Visp	1993	4	216	646	531	552	9	22
23	Volketswil	1975	39	2031	515	1178	576	10	19
24	Vétroz	1991	3	14	477	555	594	10	12
25	Wila	1990	4	69	573	1372	560	9	27
26	Wilchingen	1968	35	453	413	964	570	9	20
27	Worben	1976	1	247	435	1033	593	10	14
28	Zürich	1972	11	309	411	1123	594	10	17

Table 1: Overview of the meteorological, topographical, and aquifer conditions of all monitoring wells. DTW=Depth to Water Table [m]; DTR=Distance to river [m]; Alt=Altitude [m]; Prec=Precipitation [mm/a]; Evap=Potential evaporation [mm/a]; Temp=Average Annual Temperatures [^{o}C]; Snow=Number of annual snowy days [days].

groundwater recharge. The depth to the water table (DTW), calculated as the vertical distance between the land surface and the average measured head, varies between approximately 1 and 78 meters. The locations cover a wide range of altitudes, with high-alpine aquifers (max. 1702 m) in the southeast and large alluvial aquifers in the north (min. 277 m). Land use types consist of agricultural areas, forests, and urban areas (see Fig. 1b). All daily head time series start in 2005 or earlier (see also Table 1), and the heads are still being recorded at the time of writing as part of an active monitoring network. A summary of the hydrogeological and meteorological conditions at each location is provided in Table 1.

2.2. Meteorological and river stage data

Daily precipitation and temperature data for the location of each monitoring well for the period 1990-2020 are taken from gridded data sets (RhiresD and TabsD) provided by MeteoSwiss (MeteoSwiss, 2022). The long-term averages are shown in Table 1. Daily potential evaporation is calculated from the temperature data using the Hamon method (Hamon, 1961), as imple-

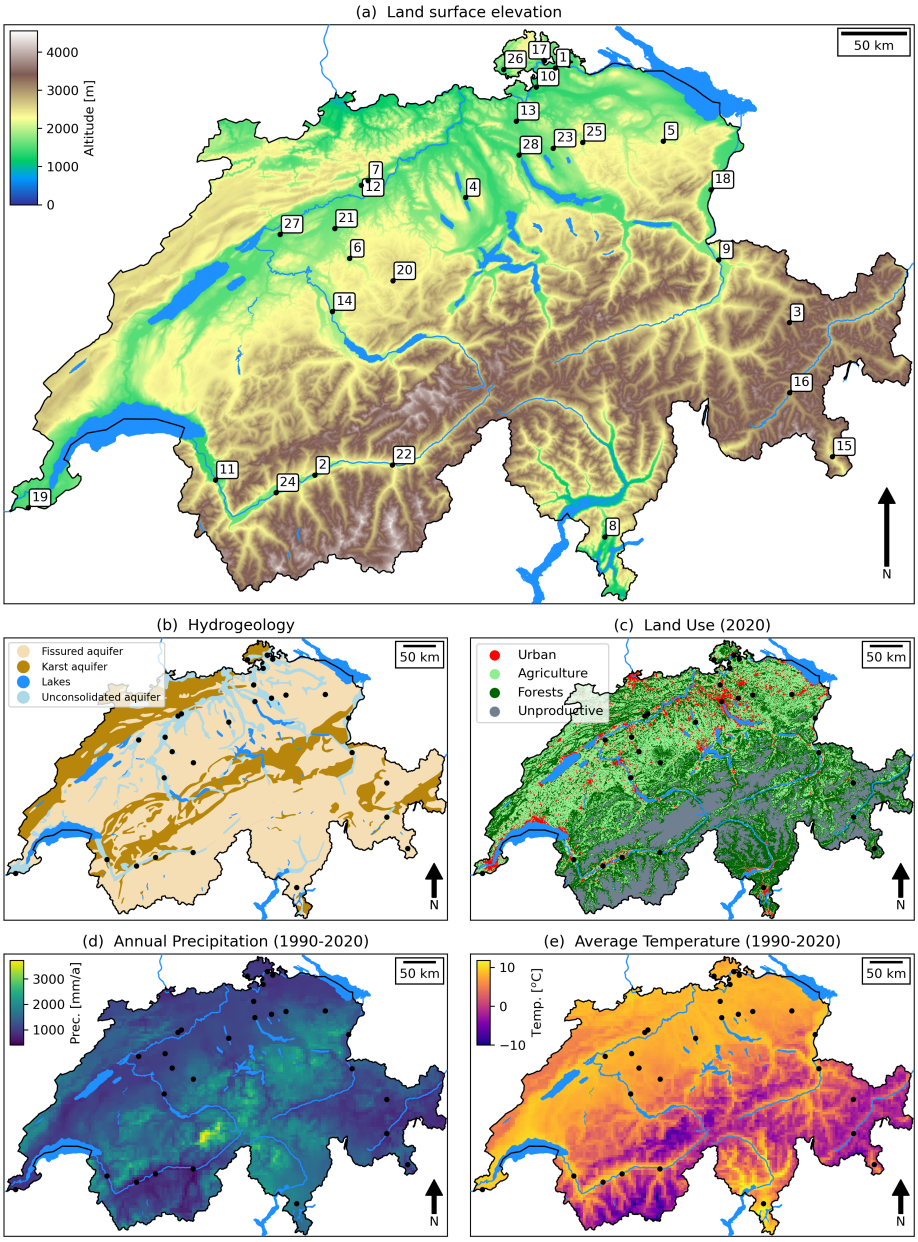

Figure 1: Overview of the locations of the monitoring wells and the hydrogeological and meteorological conditions. The numbers in map (a) relate to the ID for each location in Table 1.

mented in the Python package PyEt (Vremec and Collenteur, 2022). The mean annual precipitation ranges from approximately 531 mm/a in Visp to 1703 mm/a in Lamone, and the mean annual potential evaporation ranges from 436 mm/a in Davos to 830 mm/a in Schaffhausen in Northern Switzerland. The mean annual temperature ranges from around 2 ^{o}C in Samedan to 12 ^{o}C in Lamone. The average number of potential snow days per year, defined as the number of days with precipitation where the average daily temperature drops below 0 ^{o}C, ranges between 4 and 94 days per year in Lamone and Davos, respectively. The wide range of meteorological conditions is also observed in Fig. 1d and Fig. 1e.

Many of the measured head fluctuations are potentially affected by fluctuations in the stages from nearby rivers (see column DTR in Table 1). For each monitoring well, it was visually checked if a river stage monitoring gauge was within reasonable distance (a few kilometers) using the `hydromaps.ch` platform (accessed 2022/03/01). River stage data is obtained for 19 out of 28 groundwater monitoring wells. Most of the data (14 monitoring stations) are obtained from the national monitoring network operated by the FOEN. For five locations, the river stage data were acquired from the local Cantonal authorities. An overview of the selected rivers and data is available in the supplementary materials. The data was re-sampled to daily river stage fluctuations by averaging the hourly values and normalized by subtracting the minimum measured river stage from the time series. The data for Lamone does not cover the entire simulation period, which may affect the ability of the model to estimate the effect of the river on the heads at these locations.

3. Methods

3.1. Lumped-parameter groundwater model

A lumped-parameter groundwater model is used to simulate the head time series. Specifically, we use the method of impulse response functions, as proposed by von Asmuth et al. (2002). In this method, predefined impulse response functions are used to describe how the head responds to different stresses. All models are implemented in Pastas (Collenteur et al., 2019, v0.22.0b), an open source Python package to perform time series analysis on groundwater data. The basic model structure is as follows:

$$h(t) = \sum_{m=1}^{M} h_m(t) + d + r(t) \tag{1}$$

where $h(t)$ [L] are the measured heads, $h_m(t)$ [L] is the contribution of stress m to the head fluctuations (M stresses in total), d [L] is the base elevation of the model, and $r(t)$ [L] are the model residuals.

The contributions from different stresses (h_m) are computed using different model subroutines, named stress models in Pastas. Each stress model transforms one or more stress time series (e.g., precipitation, river stage) into a single head contribution. In this way, it is possible to decompose head time series into individual contributions from different stresses. Two stress models are used in this study, one to account for precipitation and evaporation, and one to account for surface water fluctuations. These two different stress models are described in detail in the sections below.

3.2. Effect of precipitation and evaporation

Different approaches are available from the literature to take precipitation and potential evaporation into account. In this study, three different models are applied and compared, named model structures M1, M2, and M3 and described in detail below. From model M1 to M3, the models increase in complexity of the processes included and the number of parameters. Each of these three models computes the contribution from precipitation and potential evaporation in two steps. In the first step, a single stress (a recharge flux (R)) is computed from the precipitation and potential evaporation. In the second step, the final contribution to the head fluctuations is computed by convolution R with an impulse response function following von Asmuth et al. (2002):

$$h_m(t) = \int_{-\infty}^{t} R(\tau)\theta_r(t-\tau)d\tau \tag{2}$$

where θ_r is the impulse response function that describes how the head responds to recharge pulses. In this study, a scaled gamma response function (see e.g., Collenteur et al., 2019) is used to simulate the head response to groundwater recharge or precipitation excess. The shape of the response function is determined by three parameters that need to be estimated (A, n, and a), as is visualized in Fig. 2.

3.2.1. M1: Linear model

The first approach uses a linear model to compute R in a simple way from precipitation (P) and potential evaporation (E_t) as follows:

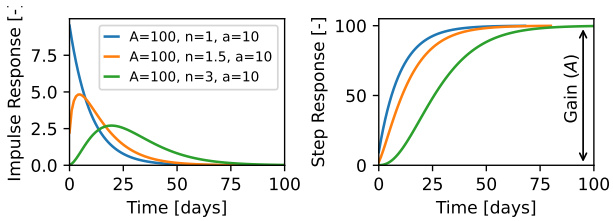

Figure 2: Examples of response functions, illustrating the effect of the parameter n on the shape of the impulse response (left) and the step response (right). The step response is the integral of the impulse response function over time.

$$R = P - fE_t \tag{3}$$

where f is an evaporation factor to update the potential evaporation to the local conditions. An advantage of this model is that only one parameter needs to be estimated (f), apart from the parameters of the response function. This comes at the cost of a highly simplified representation of the unsaturated zone processes and the assumptions that 1) the heads respond linearly to precipitation and potential evaporation, independent of the state of the system, and 2) actual evaporation is not limited by water availability and occurs at the rate of f times potential evaporation. As a result, the flux R can be both positive and negative. This may for example be the case when vegetation can tap into the groundwater to continue transpiration when limited soil water is available. Despite its apparent simplicity it should be noted that this model has been proven useful to solve groundwater problems in many studies, particularly in shallow groundwater systems where the depth to water table is only a few meters.

3.2.2. M2: Flex model

The second model applied in this study is the nonlinear recharge model developed in Collenteur et al. (2021). This model is based on a soil-water balance approach and comparable to the model presented in Peterson and Western (2014). In this approach, a model consisting of two connecting reservoirs is used to compute recharge to the groundwater and to account for the (threshold) nonlinear effects of interception processes and the root zone. A graphic representation of the model is shown in Fig. 3a. Only a summary description of the model is given here and we refer to Collenteur et al. (2021) for a detailed description.

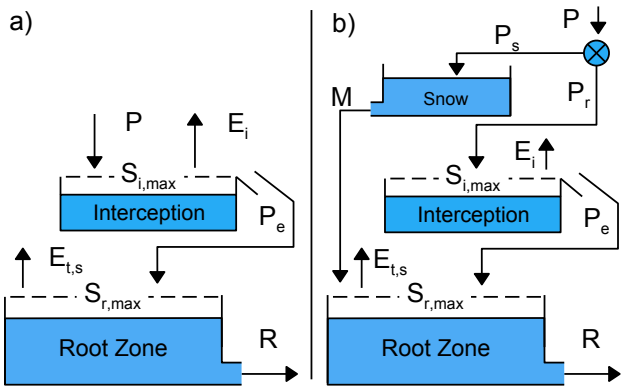

Figure 3: Conceptual recharge models applied in this study: a) the Flex model (M2) from Collenteur et al. (2021), and b) the Flex-snow model (M3) that includes an additional snow reservoir.

Precipitated water (P) exceeding the interception capacity ($S_{i,max}$) continues to the root zone storage reservoir. There, the infiltrating water is temporarily stored and released as soil evaporation and transpiration ($E_{t,s}$) or recharge to the groundwater (R). The recharge to the groundwater is computed as follows:

$$R = k_s(\frac{S_r}{S_{r,max}})^{\gamma} \tag{4}$$

where k_s [LT^{-1}] is the saturated hydraulic conductivity, $S_{r,max}$ [L] is the storage capacity of the root zone reservoir, and γ [-] is a parameter determining the nonlinearity of the recharge flux with respect to the saturation of the root zone.

An important feature of this model is that the actual evaporation is limited by the amount of available soil moisture, and evaporation stops if no soil water is available. The improved representation of hydrological processes impacting the recharge flux and ultimately the response in the heads comes at the cost of introducing additional parameters. This approach adds six parameters to the model, some of which may be fixed to sensible values. Here, the maximum interception capacity is fixed to 2 mm, and the saturation of the root zone at which actual evaporation equals potential evaporation (L_p) is fixed to $L_p = 0.25$. Parameters k_s, γ, $S_{r,max}$, and k_v (an evaporation factor) are inferred from the hydraulic head data by model calibration.

3.2.3. M3: Flex-snow model

The third applied model is developed as part of this study. This model has the same structure but extends the M2 model to take into account the effect of snowfall and snow melt on the R. The model structure presented in the previous section was developed and tested for an environment where precipitation occurs primarily as rainfall. In large parts of Switzerland, however, precipitation also occurs as snowfall. The occurrence of snowfall affects the infiltration pattern and timing, and through groundwater recharge, the head dynamics and storage. We refer to Lundberg et al. (2016) for a review of the implications of snowfall on infiltration patterns.

To account for snow processes in the calculation of groundwater recharge, the soil-water balance model described above is extended with a degree-day based snow model (e.g., Kavetski and Kuczera, 2007). The degree-day snow model was chosen because of the model simplicity but also for the shown well performance for snow melt modeling (Girons Lopez et al., 2020; Meeks et al., 2017). Moreover, we expect that the head time series may not contain enough information to infer parameters of more complex snow models. In Fig. 3b the recharge model extended with the snow reservoir is visualized.

The purpose of the snow model is to separate precipitation into snowfall and rainfall, temporarily store the snowfall, and generate snow melt when the temperature rises above a certain temperature threshold. The water balance for the snow storage reservoir is written as follows:

$$\frac{\mathrm{d}S_s}{\mathrm{d}t} = P_s - M, \tag{5}$$

where S_s [L] is the snow water storage, P_s [LT^{-1}] is the part of the precipitation that occurs as snow and M [LT^{-1}] the snow melt. Precipitation is divided into snowfall (P_s) or rainfall (P_r) as follows:

$$P_s = \begin{cases} P & \text{if } T \leq T_t, \\ 0 & \text{if } T > T_t \end{cases} \tag{6}$$

$$P_r = \begin{cases} P & \text{if } T > T_t, \\ 0 & \text{if } T \leq T_t \end{cases} \tag{7}$$

where T [Θ] is the daily mean air temperature and T_t [Θ] is the temperature below which precipitation occurs as snowfall and the temperature at which the melt starts. The snow melt (M [LT^{-1}]) is determined in a similar fashion:

$$M = \begin{cases} 0 & \text{if } T \leq T_t, \\ k(T - T_t) & \text{if } T > T_t \end{cases} \tag{8}$$

where k [LΘ $^{-1}$T^{-1}] is a factor that determines the rate of snow melt. Equation 8 is smoothed using a logistic function according to Kavetski and Kuczera (2007). In total, the snow model adds two parameters to the original recharge model (T_t and k) that need to be estimated. Here, the parameter T_t is fixed to T_t=0 ^{o}C, and only k is estimated. Apart from precipitation and potential evaporation, the extended model also requires time series of the mean daily temperature as input data. This will generally not increase input data requirements, as the temperature is required to compute the potential evaporation.

3.3. Contribution from river fluctuations

For the locations with a nearby river and related monitoring station, the river is added to the model as an additional stress. The head contribution from river stage fluctuations is computed through the convolution of a time series of measured river stages with a separate impulse response function, similar to Eq. (2). In this study, an exponential response function with two parameters (A_{riv} and a_{riv}) is used. This response function is equal to the scaled gamma response function where the parameter n is fixed to $n = 1$ (see Fig. 2).

After the model is calibrated (details below), it is checked whether the effect of the river stress can be determined with reasonable certainty and should be included in the model or not. For this purpose, the uncertainty in the estimated response function is used, applying the following criterion (e.g., Collenteur et al., 2019):

$$A_{riv} > 1.96\sigma_{A,riv} \tag{9}$$

where A_{river} is the gain of the response function (see Fig. 2) and $\sigma_{A,riv}$ is the estimated standard error of this parameters. The rationale behind this criterion is that if the gain of the response function can be inferred from the data, it is more likely that the river stress also caused (part of) the measured head fluctuations. If the above criterion is not met, the river stress is removed from the model and the model is re-calibrated. To obtain physically plausible results, the parameter A_{riv} has an upper limit of $A_{riv} = 1$, reasoning that

the rise in the head caused by the river cannot exceed the rise in the stage of the river.

3.4. Noise modeling and autocorrelation

The residual errors $r(t)$ in Eq.(1) are often found to be strongly correlated in time. For example, Marchant et al. (2016) showed that even when modeling monthly head measurements in the UK, significant autocorrelation was still present in the residuals for time lags up to 20 months. If significant autocorrelation exists, the model violates the assumption that the residuals errors are independent and normally distributed with a zero mean and a constant variance ($\sim N(0; \sigma^2)$). The consequence of violating these assumptions is that the parameter uncertainties are unreliable and may not be used. To overcome this issue, noise models can be applied to transform the residuals into uncorrelated (white) noise ($v(t)$). The commonly used auto-regressive model of order one (AR(1), e.g., von Asmuth et al., 2002) is applied for this purpose in this study. The AR(1) parameter of this model (α) determines how quickly the residual error decays and needs to be inferred from the data.

Despite the application of a noise model, the preliminary results from this study and a previous study (Collenteur et al., 2021) showed that the AR(1) noise model is generally unable to reduce the residuals to uncorrelated white noise when using daily head measurements. To still obtain models with reliable estimates of the parameter uncertainties, the original daily head measurements are resampled to lower measurement frequencies through the removal of measurements. Thirty sub-samples are taken from each original head time series, by gradually increasing the time interval between head measurements from 1 day to 30 days. Models are created and calibrated for each of these 30 sub-samples and the resulting noise time series are checked for autocorrelation. This approach allows for the systematic analysis of the effect of decreasing temporal resolution of the head measurements on the autocorrelation in the noise and the estimated model parameters and uncertainties.

The models are checked for autocorrelation for the first 15 time lags using the Ljung-Box test adapted for non-equidistant time series (Stoffer and Toloi, 1992). This tests the Null-hypothesis (H_0) that the noise errors are independent against the alternative hypothesis (H_a) that the errors are not independent. If the p-value is above a chosen significance level ($\alpha = 0.05$), it is concluded that H_0 cannot be rejected and there is no significant autocorrelation in the noise errors. For each of the model structures, the model

Model	Param.	Units	Bounds	Fixed
Base	d	m	-	μ_r
Recharge response	A	-	[1e-9, ∞]	
	a	d	[1e-2, 2e3]	
	n	-	[1e-2, 1e2]	
M1	f	-	[-1.5, -0.5]	
M2/M3	k_v	-	[0.5, 1.5]	
	$s_{i,max}$	mm	-	2
	$s_{r,max}$	mm	[1e-5, 1e3]	
	k_s	mm/d	[0, 1e4]	
	l_p	-	-	0.25
	γ	-	[1e-5, 20]	
M3	t_t	^{o}C	-	0
	k	mm/^{o}C/d	[1, 20]	
River	A_{riv}		[0, 1]	
	a_{riv}	d	[1e-2, ∞]	
Noise	α	d	[1e-9, 5e3]	

Table 2: Model parameters, units, and the boundaries used for the models. μ_r is the mean of the residuals.

calibrated to head data with the highest temporal resolution but without significant autocorrelation is selected. If a model structure has significant autocorrelation for all temporal resolutions of the head data, the model with the lowest temporal resolution (Δt=30 days) is used.

3.5. Model calibration, evaluation, and selection

Depending on the model structure (e.g., M1-M3, with or without a river) between 5 and 10 parameters need to be inferred from the head data. An overview of the model parameters is provided in Table 2. The parameters are estimated by minimizing the sum of the weighted noise criterion, following von Asmuth et al. (2002). A two-stage calibration strategy is applied, following Collenteur et al. (2021). First, the model is calibrated without a noise model, effectively minimizing the sum of the squared residuals (r). Then, the parameter determining the size of the root zone reservoir ($s_{r,max}$) is fixed, as this parameter was found to be difficult to estimate while simultaneously estimating the parameters of the noise model. In the second calibration, the noise model is added and all parameters (except $s_{r,max}$) are estimated simultaneously, using the optimal parameter values found in the first calibration as initial parameters. This strategy was found effective to obtain a good overall fit between the simulated and measured heads, while using a noise model.

The head data is divided into twelve years of data used for calibration and six years of data used for model evaluation. The evaluation data is used

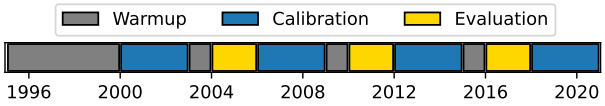

Figure 4: Calibration and model evaluation scheme applied in this study. The data from the twelve years 2000-2002, 2007-2009, 2012-2015, and 2018-2021 are used for model calibration and the six years 2004, 2005, 2010, 2011, 2016, and 2017 are used for model evaluation.

to select the model structure for each monitoring well that best describes the measured heads throughout the entire observation period (2000-2021). In that sense, it should be noted that the evaluation period is not used to demonstrate "*the model ability to perform outside of its training period*" (Arsenault et al., 2018), as it is also commonly understood. We are interested in identifying the processes (as represented in M1, M2, and M3) that need to be taken into account to simulate the entire range of the measured heads for our data set, and selecting a single model using independent head data.

Some of the head time series show particularly low heads in the last couple of years (possibly as a result of recent droughts), which are outside the historic range in the preceding period. We therefore refrained from the classical split-sample setup using a calibration period followed by an evaluation period. Instead, we opted for an odd/even type of approach (see, for example, Arsenault et al., 2018), with alternating calibrating and evaluation periods (as shown in Fig. 4). The calibration and evaluation periods are separated by a warm-up period of one year to ensure the evaluation data is independent from the calibration data. This approach for the split-sample test makes the selection less dependent on a specific period (e.g., the last six years), and more on the overall fit during different periods throughout the entire period of interest (2000-2020).

The aforementioned three model structures are tested for each of the 28 monitoring wells. The final model structure for each monitoring well is selected based on the evaluation using four goodness-of-fit metrics computed over the evaluation periods. The following goodness-of-fit metrics are used: the Mean Absolute Error (MAE), the Nash-Sutcliffe Efficiency (NSE), the Kling-Gupta Efficiency (KGE, Kling et al., 2012), and the Root Mean Squared Error (RMSE). It should be noted that changing the temporal resolution of the head data used for model calibration may mask deficiencies of the lumped-parameter model to reproduce the daily measured dynamics.

To prevent this and still allow comparison of different model structures, all goodness-of-fit metrics reported in this study to evaluate the models were computed using the original daily head data. For each metric the three models are ranked (1 for best, 3 for worst) and the final rank for each model is computed by summing the rank for the individual metrics. For each monitoring well the model with the lowest rank is selected for further analysis.

4. Results

4.1. Head data used for calibration

We first analyze the effect of using head data with different temporal resolutions to calibrate the models on 1) the model performance, 2) the autocorrelation in the noise, and 3) the estimated confidence intervals. The Nash-Sutcliffe efficiency (NSE) for the evaluation period for each model and temporal resolution of the head data is plotted in Fig. 5. We reiterate here that the metrics are computed using the original daily head measurements and simulations, and are thus directly comparable. The horizontal black lines in Fig. 5 indicate the NSE of the model with the highest possible temporal resolution of the heads that still passed the autocorrelation test. For some monitoring well and model structures there may be models calibrated to head data with lower temporal resolutions that have a higher goodness-of-fit than the finally selected models (horizontal black lines), although these do not necessarily pass the autocorrelation test.

The result displayed in Fig. 5 show that the goodness-of-fit may change depending on the temporal resolution of the head data. The use of more head measurements to calibrate the model did not necessarily improve the model fit. The contrary was actually often the case, i.e. the models calibrated to less observations (green to yellow colors) often performed better than those calibrated against head time series with higher temporal resolutions (e.g., Davos for M1, and Gossau for M2 and M3). In this regard the nonlinear models M2 and M3 appeared more sensitive compared to the linear model M1 (with only one model f parameter to calibrate in addition to the impulse parameter), as visible by a larger spread in the data. Particularly the results from model structures M2 and M3 for the monitoring well in Wilchingen appear sensitive to the head data, although these models still outperform the M1 model in all cases.

The motivation to calibrate the models to head data with different temporal resolutions was to systematically study its effect on the autocorrelation

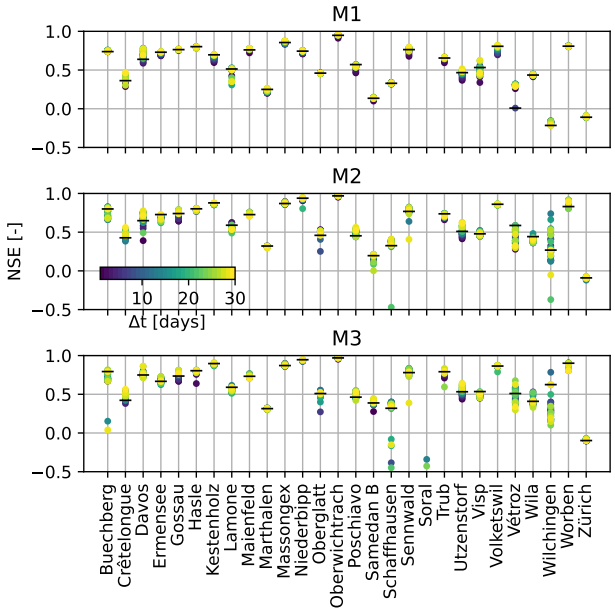

Figure 5: Nash-Sutcliffe Efficiencies (NSE) for the different model structures calibrated against head data with different temporal resolutions, ranging from 1 to 30 days between head measurements. The horizontal black lines indicate the NSE of the selected model for each model structure and monitoring well.

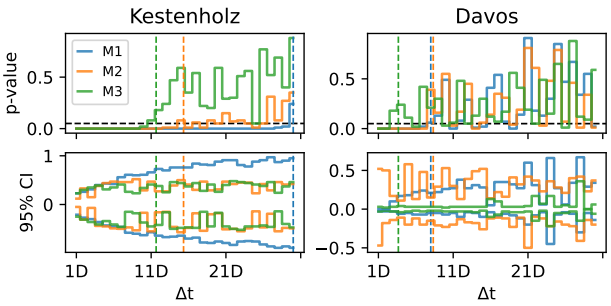

Figure 6: Examples of the effect of the temporal resolution of the head data used for calibration on the p-value of the autocorrelation test and the average width (in meters) of estimated 95% confidence intervals from the wells of Kestenholz and Davos. The vertical dashed lines indicate the temporal resolution where the model passed the autocorrelation test. The horizontal dashed lines indicate the significance level α=0.05.

and ultimately the estimated confidence intervals. Two examples of this effect are shown in Fig. 6 for the wells in Kestenholz and Davos. Plots for the other wells are shown in Fig. A.11 and Fig. A.12 in the Appendices. Both examples show how none of the models pass the autocorrelation test for high temporal resolutions (e.g., Kestenholz with resolution Δt=11 days for M3). This is also true for the remainder of the data set. More models pass the test as the temporal resolution decreases. This also affects the confidence intervals, which in most cases remain unstable until the test is passed. Particularly for head data with a high temporal resolution the confidence intervals may be both under- or overestimated compared to finally selected models without (or less) significant autocorrelation. Despite the larger number of parameters, the nonlinear models often have similar or smaller confidence intervals compared to the linear model, indicating that the additional parameters do not lead to larger model uncertainty. In general, these results show the importance of dealing with autocorrelation in the noise when estimating confidence intervals.

For further analysis, the model calibrated against the highest temporal resolution head measurements while still passing the autocorrelation test was selected for each model structure and monitoring well. The temporal resolution of the head data ranged between Δt=3 days for Davos and Lamone, and Δt=29 days for Utzensdorf, with an average of Δt=18 days. For 30 out of 84 models and for 8 out of 28 locations, no temporal resolution of the head data resulted in uncorrelated noise and lowest temporal resolution was

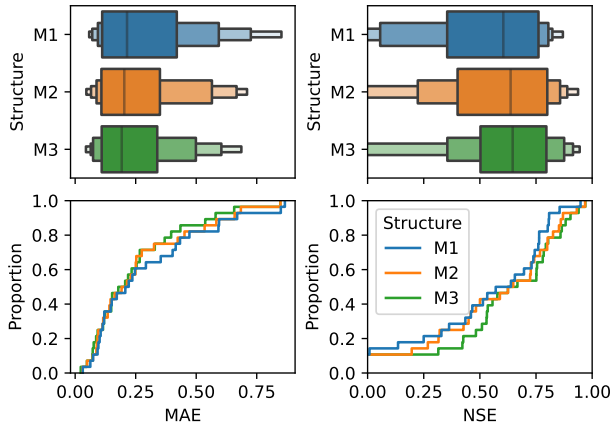

Figure 7: Extended box plots and cumulative density distributions of the goodness-of-fit metrics MAE and NSE computed over the evaluation data for all three model structures.

used (Δt=30 days). The parameter uncertainties for these models have to be interpreted with caution.

4.2. Model structure comparison

In Fig. 7 the box-plots (upper row) and cumulative density distributions (lower row) of the goodness-of-fit metrics computed over the evaluation period for the different model structures and all monitoring wells are shown. The goodness-of-fit metrics for the individual models for each monitoring well and the mean and median over all models can be found in Table A.4 in the Appendices. The results show that the nonlinear models (M2 and M3) generally outperform the linear model (M1) for the evaluation data both in terms of absolute error metrics (MAE and RMSE) and relative error metrics (KGE and NSE). For example, the median MAE drops from 0.21 to 0.19 from M1 to M3, and the median NSE increases from 0.60 to 0.65 for these model structures. It should be noted that for some wells the linear model performed better or that the improvement from the nonlinear models was only marginal. The extension of the basic nonlinear model (M2) with an snow model (M3) further improved the goodness-of-fit as measured by the NSE and MAE for the majority of the monitoring wells.

To illustrate how the inclusion of a snow model can improve the simulation of the head fluctuations, a closer look is taken at the internal dynamics of the model for the monitoring well in Davos. In Fig. 8, the measured and simulated heads, the estimated recharge, the snow storage, and the measured

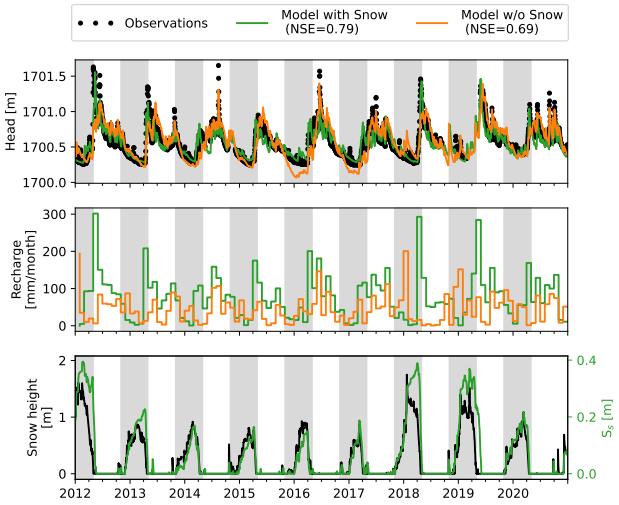

Figure 8: Simulated head fluctuations, computed recharge fluxes ($R(t)$), and snow storage state ($S_s(t)$) for the models without (M2) and with snow (M3) for the monitoring well in Davos. For comparison also the measured snow height is shown.

snow height (as a qualitative indication) are shown. The lowest heads were measured in the winter months (November-April, gray shaded areas in Fig. 8), when recharge rates are expected to be low or close to zero. In spring, when snow melts and water infiltrates, groundwater recharge increases, and a sharp rise in the head is measured. The model that included the snow reservoir simulated this measured behavior well, whereas the model without snow melt seemed unable to reproduce the measured dynamics in the head. The simulated dynamics of snow storage (lower panel in Fig. 8) also corresponded well to the measured snow height in the area.

4.3. Final model structure selection

The final model structures for each monitoring well were selected using the ranks computed from the goodness-of-fit metrics. The characteristics of the selected model structure for each monitoring well and the corresponding goodness-of-fit metrics for the calibration and evaluation periods are presented in Table 3. Plots of the measured and simulated heads for all monitoring wells are shown in Fig. A.13 in the Appendices. The M1 model was selected 4 times, the M2 model 7 times, and the M3 was selected for 17 of the 28 monitoring wells. For 15 out of 19 wells where river stage data was available, the river was maintained in the model to explain (part of) the head

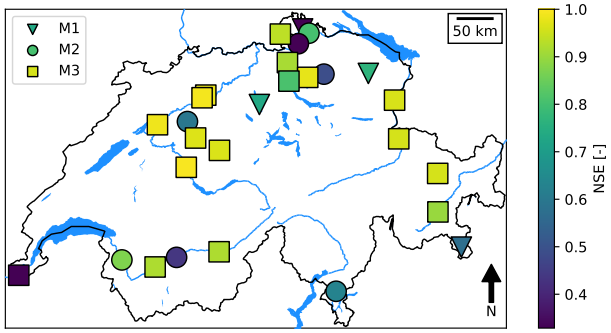

Figure 9: Map with the Kling-Gupta Efficiency in the calibration period for each model. For locations denoted by a square a snow model is present in the model, while for locations denoted by a circle no snow model is present.

fluctuations. The selected model structure and goodness-of-fit measured as the NSE in the evaluation period are also shown spatially in Fig. 9.

The selected models generally showed a reasonably good fit to the data with an average NSE of 0.70 and a median of 0.74. The goodness-of-fit varied strongly between the models with NSE values in the calibration period ranging between 0.17 and 0.97. The average model fit decreased in the evaluation period (to NSE=0.53). This average is skewed substantially, however, by two wells with poorly performing models and negative NSE values in the evaluation period (Soral and Zürich, see also Table 3). If the results from these two wells are excluded, the NSE only decreased to 0.67. For some wells the models failed to accurately simulate the head data for some individual years or periods (see for example, Zürich and Marthalen). A special case is the model for Soral, which simulates a long term trend rather than the seasonal dynamics. In the discussion we will speculate about possible reasons for under-performing models. In general, however, the results show that the majority of the observed groundwater dynamics could be satisfactorily simulated with the lumped-parameter models and the typically readily available applied stress data (precipitation, potential evaporation, and river stages).

4.4. Stresses and processes driving head fluctuations

A commonly asked question is what part of the head fluctuations can be explained by a certain stress (e.g., recharge or river stage). Quantifying the relative contribution of a stress with a single value (e.g., xx% of the head fluctuations can be explained from recharge) is not a straightforward task

	Model Structure			Importances			Calibration				Evaluation			
	dt	M	river	river	rch	unex.	MAE	RMSE	NSE	KGE	MAE	RMSE	NSE	KGE
Buechberg	30	M2	-	0.00	0.91	0.09	0.29	0.34	0.91	0.96	0.15	0.16	0.80	0.93
Crêtelongue	5	M2	Yes	0.39	0.10	0.51	0.12	0.14	0.43	0.61	0.09	0.11	0.43	0.76
Davos	3	M3	-	0.00	0.78	0.22	0.08	0.11	0.78	0.80	0.08	0.10	0.75	0.76
Ermensee	30	M1	Yes	0.30	0.49	0.21	0.28	0.37	0.80	0.89	0.25	0.34	0.73	0.69
Gossau	9	M1	-	0.00	0.75	0.25	0.20	0.26	0.74	0.78	0.21	0.26	0.76	0.77
Hasle	30	M3	Yes	0.47	0.30	0.23	0.09	0.12	0.74	0.82	0.07	0.09	0.80	0.89
Kestenholz	11	M3	-	0.00	0.95	0.05	0.21	0.25	0.96	0.97	0.25	0.32	0.88	0.94
Lamone	3	M2	Yes	0.07	0.73	0.19	0.14	0.19	0.79	0.70	0.14	0.19	0.63	0.56
Maienfeld	8	M3	Yes	0.76	0.09	0.16	0.19	0.23	0.87	0.87	0.23	0.28	0.75	0.77
Marthalen	30	M2	-	0.00	0.39	0.61	0.21	0.27	0.43	0.51	0.33	0.40	0.32	0.31
Massongex	14	M2	Yes	0.83	0.06	0.11	0.13	0.16	0.87	0.84	0.11	0.14	0.87	0.84
Niederbipp	21	M3	-	0.00	0.96	0.04	0.21	0.27	0.95	0.96	0.21	0.24	0.94	0.96
Oberglatt	30	M3	Yes	0.15	0.43	0.42	0.64	0.82	0.37	0.66	0.66	0.78	0.51	0.58
Oberwichtrach	5	M3	Yes	0.70	0.27	0.03	0.05	0.06	0.97	0.98	0.05	0.06	0.97	0.97
Poschiavo	11	M1	Yes	0.20	0.31	0.49	0.17	0.22	0.48	0.56	0.11	0.15	0.57	0.67
Samedan B	22	M3	-	0.00	0.42	0.58	0.39	0.50	0.37	0.36	0.37	0.46	0.43	0.36
Schaffhausen	23	M1	Yes	0.35	0.19	0.45	0.07	0.09	0.63	0.70	0.12	0.14	0.33	0.35
Sennwald	9	M3	Yes	0.37	0.33	0.29	0.10	0.14	0.67	0.73	0.09	0.12	0.78	0.83
Soral	30	M3	-	0.00	0.63	0.37	0.54	0.66	0.72	0.87	0.85	0.96	-2.75	-0.16
Trub	10	M3	-	0.00	0.77	0.23	0.20	0.27	0.74	0.72	0.18	0.22	0.78	0.72
Utzenstorf	23	M2	-	0.00	0.62	0.38	0.26	0.33	0.59	0.75	0.25	0.32	0.59	0.67
Visp	22	M3	Yes	0.44	0.23	0.33	0.31	0.38	0.66	0.71	0.40	0.54	0.54	0.54
Volketswil	30	M3	-	0.00	0.94	0.06	0.11	0.14	0.94	0.95	0.12	0.15	0.86	0.89
Vétroz	8	M3	Yes	0.50	0.09	0.41	0.08	0.10	0.55	0.66	0.07	0.08	0.53	0.72
Wila	16	M2	Yes	0.21	0.53	0.26	0.47	0.63	0.79	0.80	0.53	0.73	0.48	0.56
Wilchingen	30	M3	-	0.00	0.79	0.21	0.68	0.84	0.74	0.84	0.43	0.58	0.62	0.83
Worben	12	M3	Yes	0.65	0.24	0.11	0.03	0.04	0.87	0.89	0.02	0.03	0.90	0.95
Zürich	17	M3	-	0.00	0.17	0.83	0.39	0.47	0.17	0.25	0.58	0.83	-0.08	0.01
Mean	-	-	-	0.23	0.48	0.29	0.24	0.30	0.70	0.75	0.25	0.31	0.53	0.67
Median	-	-	-	0.15	0.43	0.25	0.20	0.26	0.74	0.78	0.21	0.24	0.63	0.72

Table 3: Model structure and goodness-of-fit metrics for the calibration and validation period for all monitoring wells.

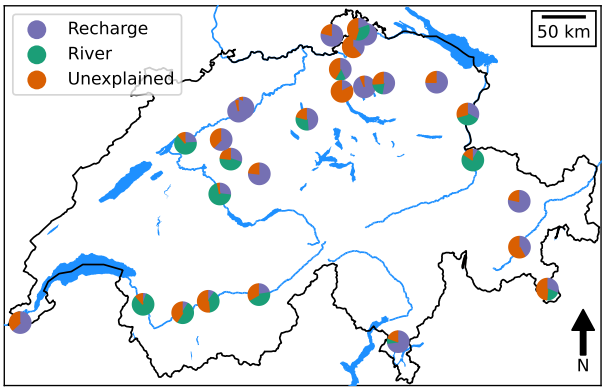

Figure 10: Relative importance of the different stresses for each well. The unexplained portion is computed as 1 - R^2.

(see, for example, Budescu, 1993, and references therein). Here, we used the dominance analysis method proposed by Budescu (1993) to quantify the relative importance of the different stresses in explaining the measured heads. In dominance analysis, the relative importance of a stress is quantified by the additional R^2 contribution from a stress, averaged over all possible subset models (e.g., including the river stress or not). The relative importance from all stresses sum up to the R^2 for the model including all stresses, making it possible to visualize the relative contributions in a pie-chart.

In Fig. 10 and Table 3 the relative importance of the different stresses for each well are shown. For 15 out of 28 monitoring wells (54%), the river stage is used to explain at least part of the head fluctuations. This shows that taking river stage fluctuations into account is important in many aquifers throughout Switzerland. For some individual wells, the relative importance of the river stages exceeds that of recharge importance (e.g., Massongex and Maienfeld). In particular, the head fluctuations measured in the Rhone valley in southeastern Switzerland (Visp, Massongex, Crêtelongue, and Vétroz) were largely explained from the fluctuations of the river stage of the Rhone river. For these monitoring wells, the depth to the water table is relatively small and they are close to the river (see Table 1). Thus, strong groundwater-surface water interaction is occurring. This strong control of the Rhone river on the groundwater dynamics in this area was also found by Schürch and Vuataz (2000), and the results from this study confirm these findings. As river stages are in many places controlled by humans, this provides an oppor-

tunity to manage the groundwater in such aquifers by controlling the river stages.

5. Discussion

5.1. Temporal resolution of the head data

The models were calibrated against 30 different head time series with decreasing temporal resolutions. Similar to Van der Spek and Bakker (2017), we found that the Nash-Sutcliffe efficiency on average slightly increased as the temporal resolution decreased. This is possibly the result of the simultaneous estimation of the parameters of the deterministic model and the noise model, which is known to sometimes lead to non-robust parameter estimation (e.g., Evin et al., 2014). In that case, the parameter(s) of the noise model are used to minimize the value of the objective function, rather than the parameters of the deterministic model, and the model parameters may not be optimal. This is particularly the case for high temporal resolutions, for which most models did not pass the autocorrelation test and subsequently were not used for further analysis.

The results from this study confirm, with a larger sample size, the finding from Collenteur et al. (2021) that the AR(1) noise model is generally unable to produce uncorrelated noise errors for time series with daily heads. Using higher resolution head data generally leads to stronger autocorrelation in the noise errors. This finding, along with the finding that using higher temporal resolutions does not necessarily lead to better model performances, is not entirely unexpected. The existence of autocorrelation indicates that there are fewer independent measurements than the number of measurements in the time series, and we are thus overestimating the effective sample size. Using head data with a lower temporal resolution for model calibration therefore does not necessarily imply that less information is available in the data to infer the model parameters, possibly explaining why model performances remain relatively similar. Using too few measurements may, however, impede the ability to infer certain parameters. For example, Kavetski et al. (2011) showed that the inference of parameters that are responsible for fast processes improves when using a temporal resolution that matches the time scale of the process.

Testing the use of different temporal resolutions of the calibration data was ultimately done to obtain reliable estimates of the parameter uncertainties and associated confidence intervals. The results showed that the

estimated confidence intervals are not constant throughout the different calibrations and can change substantially depending on the temporal resolution of the head data used for calibration. For some models, often with low goodness-of-fit, the confidence intervals are wide and/or unstable (e.g., Soral, Schaffhausen, and Visp), indicating the parameters for these models are uncertain and could not be estimated reliably. In many cases, the width of the confidence intervals increases with decreasing temporal resolution of the head data (see, for example, Kestenholz, Oberglatt, and Niederbipp). Thus, when using head data with high temporal resolutions and not passing autocorrelation tests, there is a high change of (severely) underestimating the parameter uncertainty.

In summary, changing the temporal resolution of the head data used for model calibration generally has little impact on the model goodness-of-fit, but may lead to substantially different confidence intervals due to the violation of the assumption on the noise errors being uncorrelated. Application of the currently available models to high resolution head data generally leads to a violation of the basic statistical assumptions underlying commonly used uncertainty quantification techniques (e.g., $\sim N(0; \sigma^2)$). Given the fact that head time series with high temporal resolutions are now widely available, there is an urgent need for more research on how to robustly quantify parameter uncertainties when calibrating models to such head data. Until such techniques emerge, the use of head data with lower temporal resolution to calibrate models is recommended.

5.2. Selecting appropriate model structures

Different model structures to account for precipitation and evaporation were tested for each monitoring well in this study. A single model structure was selected using the average rank of the models from four different goodness-of-fit metrics. This means that all goodness-of-fit metrics weigh equally. Criteria such as the Bayesian or Akaike Information criterion could not be used, as the different model structures may be calibrated to head data with different temporal resolutions and the number of error values in the noise time series strongly affects such criteria. The goodness-of-fit metrics, however, could be computed using the daily head measurements and simulations, and was therefore used. The models always simulate the heads with a daily time step, regardless of the temporal resolution of the head data used for model calibration. As a result of these choices, no penalty was given for the number of parameters in the models. If the number of parameters is

taken into account this might benefit the M1 model, which has less parameters that need to be estimated. In this regard, it could be investigated if more formal model selection strategies, such as Bayesian model selection as outlined in Marshall et al. (2005), would yield different or similar results.

Whether or not to include the river in the final model was decided using the uncertainty of the response function (see Eq. (9)). Such an approach has also been applied in other studies to determine if a stress is influencing the heads or not, for example for pumping wells (Collenteur et al., 2019; Brakenhoff et al., 2022). For five monitoring wells (Ermensee, Oberglatt, Poschiavo, Visp, and Wila), the parameter for the gain of the response to river stage changes (A_{riv}) was estimated at the upper boundary value of $A_{riv} = 1$. The estimated parameter uncertainty may not be reliable because of this, which possibly affects the applicability of the applied criteria. To investigate the impact of possibly incorrectly keeping the river stress in the model, the models for these five monitoring wells were compared to the same (re-calibrated) models after deleting the river stress. The results from this analysis (see Fig. A.14 in the Appendices) show that deleting the river stress from the model decreases model performance in the evaluation period for all models. However, visual inspection of the simulated heads shows that these differences are only marginal for all wells but Visp.

As noted by Shapoori et al. (2015a), it is generally assumed that models with a good fit can be used to decompose the head time series into contributions of different stresses, and that the estimated contributions represent the true contributions, with some uncertainty. This assumption was implicitly also made in this study, for example to compute the relative contributions shown in Fig. 10. The analysis described above shows that this assumption may not always be valid, as there are different model structures with comparable fits but with fundamentally different hydrological processes generating the simulated head dynamics. The result thus strongly depends on the model selection criteria. A confounding factor for this assumption here is that both river stages and recharge are dependent on precipitation and evaporation and are thus correlated to at least some extent. If it rains, both recharge and river stages tend to increase, which may reduce our ability to decompose the contributions of these two stresses without adding additional information to better inform the model.

The finding that for these five monitoring wells there are multiple model structures that perform almost equally well to simulate the heads, only came to light after this additional analysis. A multi-model approach, as for exam-

ple is taken in Brakenhoff et al. (2022) as well as in this study for the snow model, would have revealed this issue at an earlier stage and is therefore recommended for future studies. This way, additional criteria can be used to make a more informed decision and to determine which model is best and used for further analysis. It may well be that additional information from independent data sources (e.g., water quality or isotopic data) is required to reliably decompose the contributions of these two stresses.

5.3. Modeling heads in Switzerland

The results from this study show that taking additional (nonlinear) processes into account in the model (as presented in M2 and M3) generally improves the simulation of the heads compared to the linear model (M1). This finding adds to the growing body of literature showing that nonlinear models can improve the simulation of the heads (e.g., Peterson and Western, 2014; Shapoori et al., 2015b; Collenteur et al., 2021), and should be considered more often. The improved performance comes at the expense of additional model parameters compared to linear models, but that does not necessarily result in wider confidence intervals (see the example of Davos in Fig. 6). This is in line with Moeck et al. (2018), which shows that additional parameters do not lead necessary to larger model uncertainty and the model structure can be more important than the amount of parameters and model calibration approach. An additional advantage of using such nonlinear models is that the results are more physically interpretable, and can for example be used to estimate groundwater recharge (e.g., Collenteur et al., 2021). For pure head prediction purposes, however, the linear model may suffice or even be preferred for individual wells, as shown by the four models in this study where the linear model outperformed the nonlinear models. This result also highlights the benefits of an individual assessments of which model structure best works for each well.

If a single model structure is to be chosen for Switzerland, for example to ensure model inter-comparability, the model structure M3 would be recommended here based on the results of this study. The inclusion of snow processes is important to simulate groundwater dynamics in Switzerland and similar cold-temperature regions. This is particularly the case in heavily snow-impacted aquifers (e.g., Davos), and the use of a degree-day snow model can substantially improve simulation results in these settings. The inclusion of a snow model increases the number of parameters but also improved process representation, which may ultimately lead to better predictions when

conditions change (e.g., warmer climate with less snowfall). The degree-day snow model was chosen because it was assumed that the head time series may not contain enough information to parameterize more complex snow models. The results from this study could be used to select monitoring wells clearly impacted by snow processes, to perform a more systematic analysis on the validity of this assumption and the applicability of more complex snow models, following, for example, Girons Lopez et al. (2020).

Despite many models achieving reasonable fits with the observed data, for some monitoring wells the lumped-parameter models performed less well. We highlight here that poorly performing models are (just as) valuable, as they inform us about our incomplete knowledge about the groundwater system causing the observed dynamics and/or how to model them. This allows us to perform a targeted search into the causes and thus improve our understanding of the groundwater system under study. Wells with particularly low performance (NSE < 0.5 during evaluation) are for example Soral, Zürich, Marthalen, Schaffhausen, and Samedan B. Assuming that the models generally work well, as exemplified by the other models, we speculate here about the possible reasons for poor model performances.

The model for Soral showed a poor performance over the entire simulation period. This may be caused by the large depth to water table (78m) and long response times not well represented in the model. However, the strong rising trend in the head is unlikely to be caused by precipitation and evaporation, as large meteorological and hydrological droughts that would have the opposite effect occurred in this last period (e.g., Brunner et al., 2019). This suggests that some unknown influence caused rising heads. The occurrence of large drought events may explain the deviations for Schaffhausen around the years 2003 and 2018. Possibly, unknown, local, and/or temporary groundwater pumping in these periods caused increased head declines, but more investigations are required to test this hypothesis. Such temporary pumping almost certainly affected the heads in Zürich between 2008 and 2012, in order to drain the construction site of the "Durchmesserlinie" tunnel built between 2008 and 2010 (Kobel, 2009). The poor performance of the model for the monitoring well in Samedan may be explained by the lack of river stage data for the nearby river Inn that likely affects the head dynamics. If data for such missing stresses is available, these could easily be added to the model to try and improve the model fit and test these hypotheses (see, for example, von Asmuth et al., 2008).

6. Analyzing nationwide monitoring networks: challenges and ways forward

As demonstrated in this study, lumped-parameter modeling using impulse response functions is a powerful method to analyze hydraulic head data observed in different hydrogeological settings, as commonly observed in nationwide monitoring networks. The models can be setup and calibrated in a limited amount of time and with low data requirements, while high accuracy predictions are often obtained. Nationwide monitoring networks typically contain more monitoring wells than the data set analyzed in this study, posing both opportunities and challenges. The workflow applied in this study may become too computationally demanding, for example when analyzing tens of thousands of time series as is done in Zaadnoordijk et al. (2019) for the Netherlands.

Depending on the purpose of modeling, different stresses can be included in the model. Particularly for nationwide networks, obtaining data for stresses other than precipitation and evaporation may be difficult and time consuming. This puts a limit on the potential performance of the models. Collecting this data, for example river stages in this study, would also be necessary for other types of models and is often a one-time exercise. The output of this exercise is valuable and may be worth the investment. This will be particularly true if the results are made publicly available for others, reducing data collection efforts for future studies. Often we do not know which stresses cause head fluctuations and, as demonstrated in this study, lumped-parameter models may be helpful in building and testing hypotheses of where other stresses or anthropogenic influences are required to model the heads. If one is interested in studying long-term groundwater trends caused by meteorological stresses only, the method can be used to select appropriate monitoring wells for this purpose.

The brute-force approach to select the temporal resolution of the head data may not always be feasible for nationwide monitoring network with more wells (as in Zaadnoordijk et al., 2019, for example). The computational demand could be reduced substantially, however, by checking for autocorrelation directly after model calibration, and decreasing the temporal resolution only if there is still significant autocorrelation present. Alternatively and much more efficiently, a fixed temporal resolution may be used, as is for example done in Brakenhoff et al. (2022). An individual approach to select the temporal resolution may, however, allow the use of more data for model cali-

bration, which potentially allows the identification of more complex models. Future research could focus on developing (empirical) rules and practical recommendations on how to select the head data used for calibration, preferably as a pre-processing step.

With increasing size of the monitoring networks, the outcomes depend more and more on the ability of the automated, reproducible workflow for the modeling to produce 'good' models for very different groundwater dynamics. Any improvements in the methods for model (structure) calibration and selection would thus benefit the final results. In the workflow presented here, the estimation of the model parameters depends for a large part on the optimization technique to find an optimum. Similarly, the selection of the model structure depends on the goodness-of-fit metrics, although other criteria may be applied there. As the size of the network increases, we also learn more about the hydrogeological and climatological settings under which certain model structures work best, and what parameters are typically found. Recent explorations to learn more about these relationships (Jemeljanova and Collenteur, 2022) have shown that relationships exist between the model parameters and hydrogeological setting, and the model structure and climatic conditions. Future research could investigate if we can exploit such relationships to make more informed decisions about (initial) parameter values and suitable model structures, depending on the characteristics of the head time series and the well setting, to further improve the modeling workflow.

7. Conclusions and outlook

The main objective of this study was to assess the applicability of lumped-parameter groundwater models to efficiently analyze data from nationwide groundwater monitoring networks. The data from 28 piezometers of the Swiss groundwater monitoring network NAQUA were used as a case study. The models were used to increase understanding of the groundwater system by investigating which stresses and processes are required to model measured head fluctuations. To this end, different model structures were tested to take precipitation and evaporation into account. To make the models applicable in snow-dominated alpine environments, the implementation of a degree-day snow model was tested in this type of model, for the first time.

The results showed that most of the head time series from the Swiss monitoring network could be modeled with high accuracy using the lumped-parameter models and only a handful of stresses for which data is com-

monly available. This demonstrates the general applicability of the model and method to simulate a wide range of groundwater dynamics. The nonlinear models (M2 and M3) generally resulted in better fits with the observed data compared to the linear model (M1), and the nonlinear model accounting for snow processes (M3) was often preferred over the nonlinear model without this process (M2). This suggests that the inclusion of snow processes is often important when modeling heads in more alpine environments. For 15 out of 28 monitoring wells the river stage was used in the model to explain part of the measured heads. This indicates the general importance of groundwater-surface water interactions when modeling groundwater dynamics throughout Switzerland. For a few monitoring wells there are signs that the heads may be influenced by stresses not included in this study, such as pumping. Caution is required when using the head data of these monitoring wells for investigations into long-term groundwater developments under natural conditions, e.g., resulting from climate change rather than anthropogenic influences such as pumping.

The models developed in this study were primarily used to improve the understanding of the groundwater systems in Switzerland. In future studies, the models can be used for other purposes as well, for example for the hindcasting of heads to study long-term groundwater drought developments (e.g., Brakkee et al., 2022), or the short-term forecasting of heads (e.g., Mackay et al., 2014). Apart from practical applications, more work is required to further improve the application and robustness of the presented workflow, although high accuracy in the modeled groundwater dynamics was already obtained. In this regard particularly the selection of the head data used for model calibration needs more detailed research.

Acknowledgments

This work was funded by the Austrian Science Fund (FWF) under research grant W1256 (Doctoral Programme Climate Change: Uncertainties, Thresholds and Coping Strategies).

Research Data and Software

Pre-processed data and scripts to reproduce the figures and tables from this manuscript are available from the following Zenodo repository: `https://doi.org/10.5281/zenodo.7494481`.

Declaration of Competing Interest

The authors declare that they have no conflict of interest.

CRediT authorship contribution statement

Raoul A. Collenteur: Conceptualization, Methodology, Data Curation, Software, Writing - Original Draft. Christian Moeck: Conceptualization, Methodology, Data Curation, Writing - Review & Editing. Mario Schirmer: Conceptualization, Writing - Review & Editing, Supervision. Steffen Birk: Supporting Conceptualization, Writing - Review & Editing, Funding acquisition, Supervision.

Appendix A. Figures and Tables

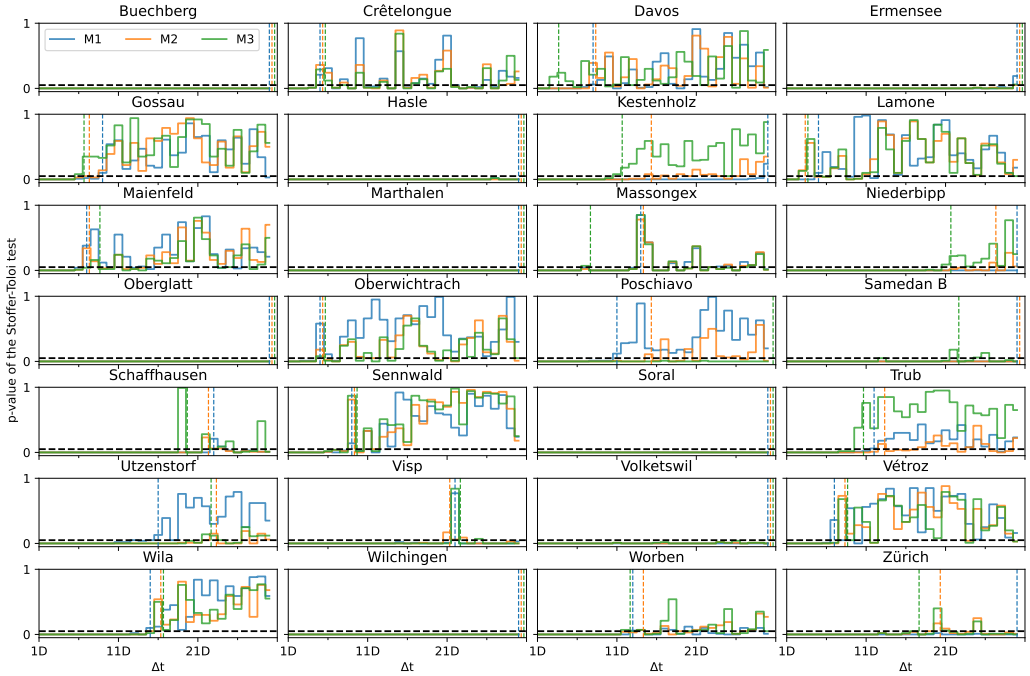

Figure A.11: Effect of the temporal resolution of the head measurements on the autocorrelation in the noise, measured as the p-value of the Stoffer-Toloi autocorrelation test. The vertical dashed lines indicate the temporal resolution where the model passed the autocorrelation test. The horizontal dashed lines indicate the significance level α=0.05.

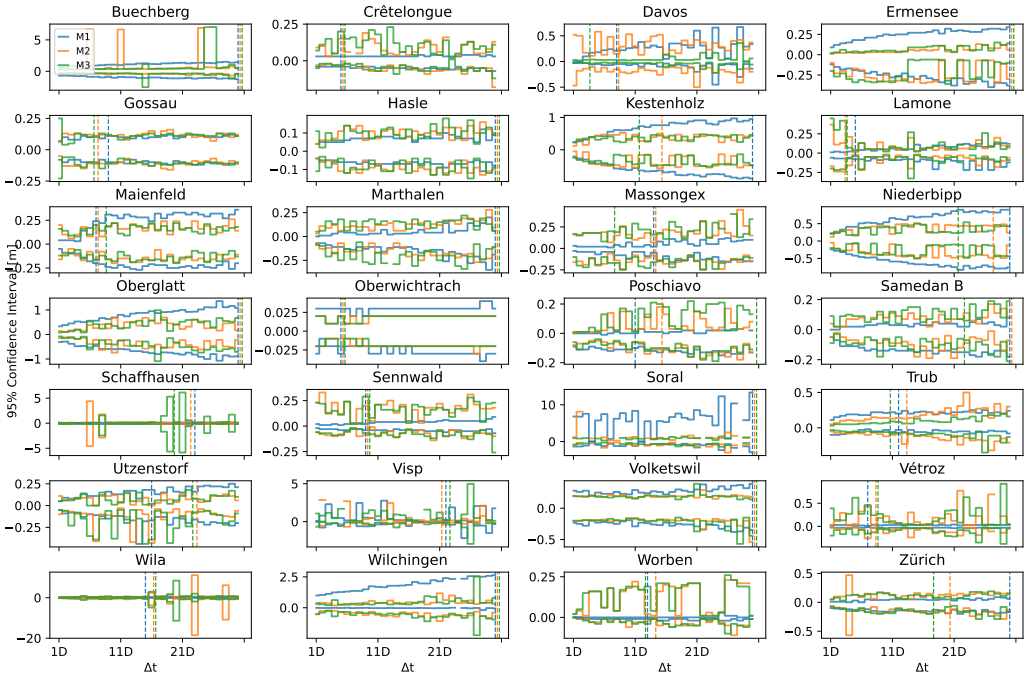

Figure A.12: Widths of the 95% confidence intervals (in meters, normalized around zero) for each monitoring well and all temporal resolutions of the head data. The vertical dashed lines indicate the temporal resolution where the model passed the autocorrelation test. Note that the confidence interval was computed neglecting any autocorrelation in the noise, if any, which means that they may be poor estimates.

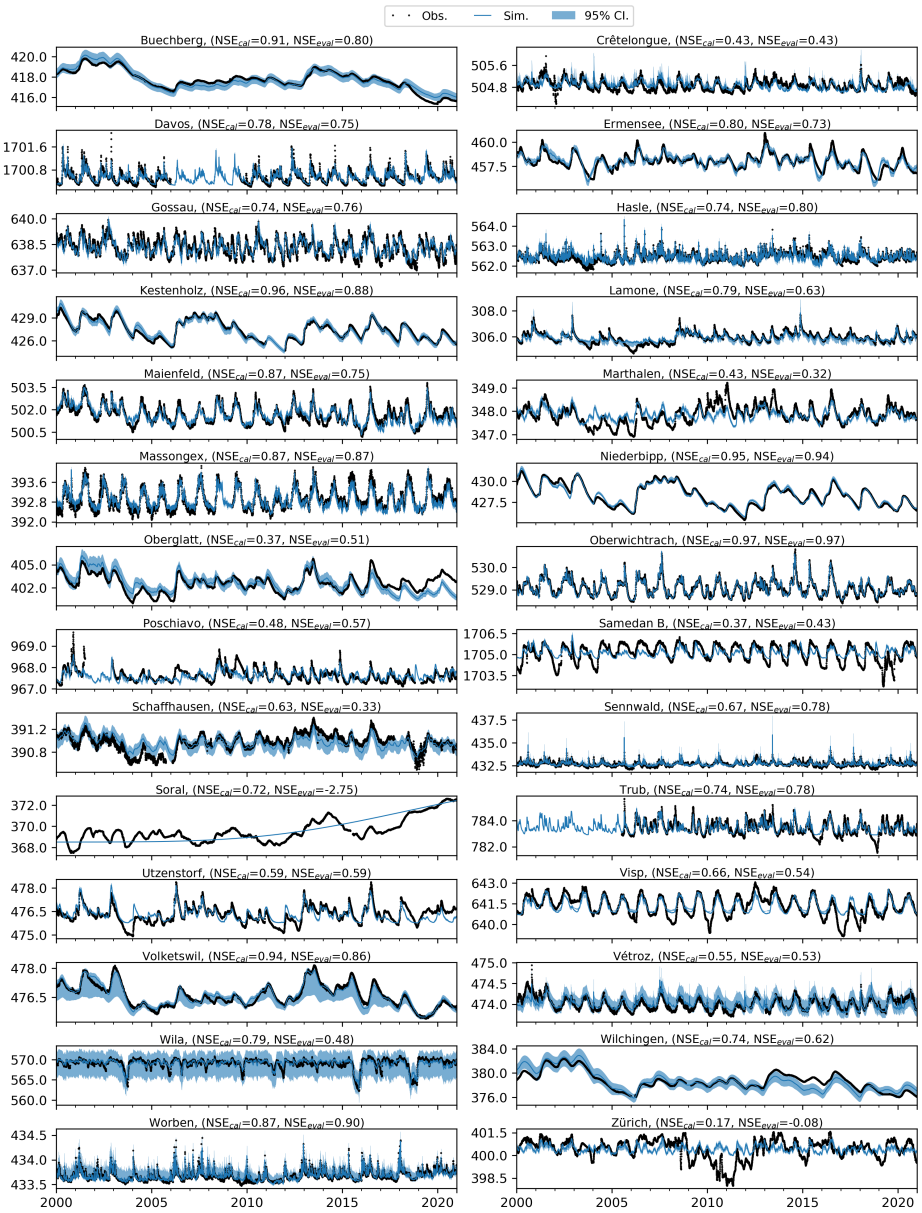

Figure A.13: Measured and simulated heads for all monitoring wells. The shaded area denotes the 95% confidence intervals of the models.

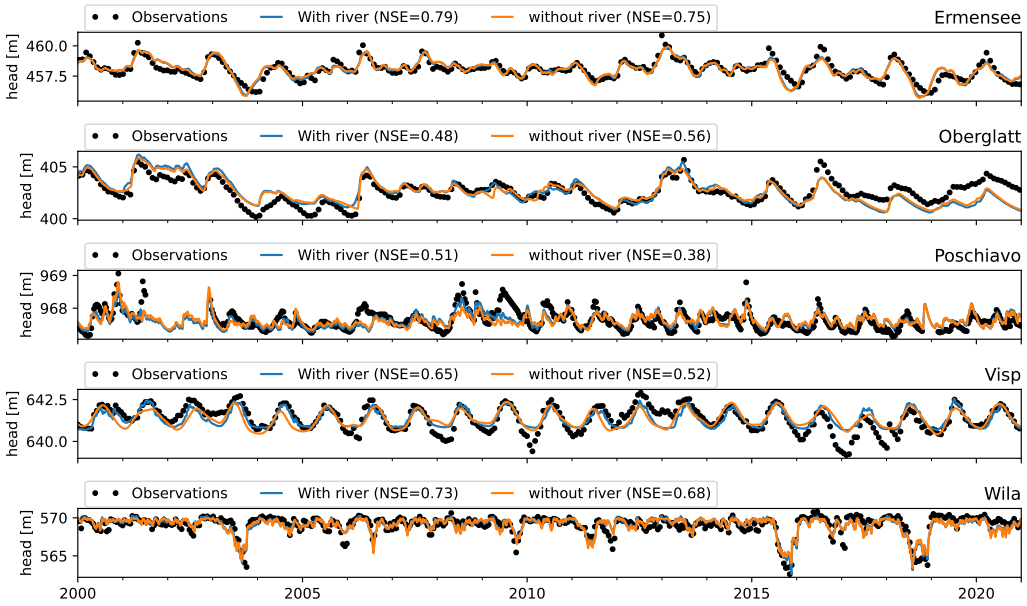

Figure A.14: Comparison of selected models with and without a river stress in the model to explain the head fluctuations.

Metric			MAE			RMSE			NSE			KGE
Structure	M1	M2	M3	M1	M2	M3	M1	M2	M3	M1	M2	M3
Buechberg	0.15	0.15	0.15	0.19	0.16	0.17	0.74	0.80	0.79	0.93	0.93	0.94
Crêtelongue	0.10	0.09	0.09	0.11	0.11	0.11	0.36	0.43	0.42	0.74	0.76	0.76
Davos	0.10	0.10	0.08	0.12	0.12	0.10	0.64	0.65	0.75	0.70	0.72	0.76
Ermensee	0.25	0.25	0.27	0.34	0.34	0.38	0.73	0.73	0.67	0.69	0.64	0.65
Gossau	0.21	0.23	0.22	0.26	0.28	0.26	0.76	0.72	0.75	0.77	0.76	0.75
Hasle	0.07	0.07	0.07	0.09	0.09	0.09	0.80	0.80	0.80	0.88	0.88	0.89
Kestenholz	0.43	0.28	0.25	0.51	0.36	0.32	0.70	0.85	0.88	0.74	0.93	0.94
Lamone	0.17	0.14	0.15	0.21	0.19	0.20	0.51	0.63	0.58	0.63	0.56	0.53
Maienfeld	0.24	0.25	0.23	0.27	0.29	0.28	0.76	0.73	0.75	0.76	0.76	0.77
Marthalen	0.35	0.33	0.33	0.42	0.40	0.40	0.25	0.32	0.31	0.24	0.31	0.31
Massongex	0.12	0.11	0.12	0.15	0.14	0.15	0.86	0.87	0.86	0.81	0.84	0.79
Niederbipp	0.42	0.21	0.21	0.50	0.26	0.24	0.74	0.93	0.94	0.80	0.95	0.96
Oberglatt	0.67	0.68	0.66	0.82	0.82	0.78	0.46	0.46	0.51	0.60	0.53	0.58
Oberwichtrach	0.06	0.05	0.05	0.08	0.06	0.06	0.95	0.97	0.97	0.98	0.97	0.97
Poschiavo	0.11	0.13	0.12	0.15	0.17	0.16	0.57	0.45	0.53	0.67	0.58	0.60
Samedan B	0.47	0.45	0.37	0.56	0.54	0.46	0.14	0.20	0.43	0.04	0.12	0.36
Schaffhausen	0.12	0.16	0.15	0.14	0.21	0.18	0.33	-0.47	-0.08	0.35	0.20	0.20
Sennwald	0.09	0.09	0.09	0.12	0.12	0.12	0.76	0.77	0.78	0.78	0.83	0.83
Soral	0.85	0.85	0.85	0.96	0.96	0.96	-2.77	-2.76	-2.75	-0.17	-0.16	-0.16
Trub	0.22	0.19	0.18	0.28	0.24	0.22	0.66	0.74	0.78	0.69	0.72	0.72
Utzenstorf	0.29	0.25	0.27	0.37	0.32	0.34	0.47	0.59	0.56	0.64	0.67	0.62
Visp	0.40	0.42	0.40	0.55	0.56	0.54	0.53	0.50	0.54	0.54	0.48	0.54
Volketswil	0.15	0.12	0.12	0.18	0.15	0.15	0.81	0.86	0.86	0.83	0.88	0.89
Vétroz	0.11	0.09	0.07	0.12	0.10	0.08	0.01	0.32	0.53	0.33	0.68	0.72
Wila	0.59	0.53	0.54	0.76	0.73	0.73	0.44	0.48	0.48	0.50	0.56	0.56
Wilchingen	0.87	0.66	0.43	1.05	0.81	0.58	-0.22	0.27	0.62	0.54	0.70	0.83
Worben	0.03	0.03	0.02	0.04	0.04	0.03	0.81	0.83	0.90	0.83	0.87	0.95
Zürich	0.59	0.58	0.58	0.84	0.84	0.83	-0.11	-0.09	-0.08	-0.04	-0.00	0.01
Median	0.21	0.20	0.19	0.26	0.25	0.23	0.60	0.64	0.65	0.69	0.71	0.73

Table A.4: Goodness-of-fit metrics for the evaluation data for the three different model structures for all monitoring wells.

References

Arsenault, R., Brissette, F., Martel, J.L., 2018. The hazards of split-sample validation in hydrological model calibration. Journal of Hydrology 566, 346–362. URL: https://www.sciencedirect.com/science/article/pii/S0022169418307145, doi:10.1016/j.jhydrol.2018.09.027.

von Asmuth, J.R., Bierkens, M., Maas, K., 2002. Transfer function-noise modeling in continuous time using predefined impulse response functions. Water Resources Research 38, 23–1–23–12. URL: https://agupubs.onlinelibrary.wiley.com/doi/abs/10.1029/2001WR001136, doi:10.1029/2001WR001136.

von Asmuth, J.R., Maas, K., Bakker, M., Petersen, J., 2008. Modeling Time Series of Ground Water Head Fluctuations Subjected to Multiple Stresses. Groundwater 46, 30–40. URL: https://onlinelibrary.wiley.com/doi/full/10.1111/j.1745-6584.2007.00382.x, doi:10.1111/j.1745-6584.2007.00382.x.

Babre, A., Kalvāns, A., Avotniece, Z., Retiķe, I., Bikše, J., Jemeljanova, K.P.M., Zelenkevičs, A., Dēliņa, A., 2022. The use of predefined drought indices for the assessment of groundwater drought episodes in the Baltic States over the period 1989–2018. Journal of Hydrology: Regional Studies 40, 101049. URL: https://www.sciencedirect.com/science/article/pii/S2214581822000623, doi:10.1016/j.ejrh.2022.101049.

Bakker, M., Schaars, F., 2019. Solving Groundwater Flow Problems with Time Series Analysis: You May Not Even Need Another Model. Groundwater 57, 826–833. URL: https://doi.org/10.1111/gwat.12927, doi:10.1111/gwat.12927.

Brakenhoff, D.A., Vonk, M.A., Collenteur, R.A., Van Baar, M., Bakker, M., 2022. Application of Time Series Analysis to Estimate Drawdown From Multiple Well Fields. Frontiers in Earth Science 10. URL: https://www.frontiersin.org/article/10.3389/feart.2022.907609, doi:10.3389/feart.2022.907609.

Brakkee, E., van Huijgevoort, M.H.J., Bartholomeus, R.P., 2022. Improved understanding of regional groundwater drought development

through time series modelling: the 2018–2019 drought in the Netherlands. Hydrology and Earth System Sciences 26, 551–569. URL: https://hess.copernicus.org/articles/26/551/2022/, doi:10.5194/hess-26-551-2022.

Brunner, M.I., Liechti, K., Zappa, M., 2019. Extremeness of recent drought events in Switzerland: dependence on variable and return period choice. Natural Hazards and Earth System Sciences 19, 2311–2323. URL: https://nhess.copernicus.org/articles/19/2311/2019/, doi:10.5194/nhess-19-2311-2019. publisher: Copernicus GmbH.

Budescu, D.V., 1993. Dominance analysis: A new approach to the problem of relative importance of predictors in multiple regression. Psychological Bulletin 114, 542–551. doi:10.1037/0033-2909.114.3.542. place: US Publisher: American Psychological Association.

Collenteur, R.A., Bakker, M., Caljé, R., Klop, S.A., Schaars, F., 2019. Pastas: Open Source Software for the Analysis of Groundwater Time Series. Groundwater 57, 877–885. URL: https://doi.org/10.1111/gwat.12925, doi:10.1111/gwat.12925.

Collenteur, R.A., Bakker, M., Klammler, G., Birk, S., 2021. Estimation of groundwater recharge from groundwater levels using nonlinear transfer function noise models and comparison to lysimeter data. Hydrology and Earth System Sciences 25, 2931–2949. URL: https://hess.copernicus.org/articles/25/2931/2021/, doi:10.5194/hess-25-2931-2021.

van Dijk, W.M., Densmore, A.L., Jackson, C.R., Mackay, J.D., Joshi, S.K., Sinha, R., Shekhar, S., Gupta, S., 2019. Spatial variation of groundwater response to multiple drivers in a depleting alluvial aquifer system, northwestern India. Progress in Physical Geography: Earth and Environment , 0309133319871941URL: https://doi.org/10.1177/0309133319871941, doi:10.1177/0309133319871941.

Evin, G., Thyer, M., Kavetski, D., McInerney, D., Kuczera, G., 2014. Comparison of joint versus postprocessor approaches for hydrological uncertainty estimation accounting for error autocorrelation and heteroscedasticity. Water Resources Research 50, 2350–2375. URL: https://doi.org/10.1002/2013WR014185, doi:10.1002/2013WR014185. publisher: John Wiley & Sons, Ltd.

Girons Lopez, M., Vis, M.J.P., Jenicek, M., Griessinger, N., Seibert, J., 2020. Assessing the degree of detail of temperature-based snow routines for runoff modelling in mountainous areas in central Europe. Hydrology and Earth System Sciences 24, 4441–4461. URL: https://hess.copernicus.org/articles/24/4441/2020/, doi:10.5194/hess-24-4441-2020.

Hamon, W.R., 1961. Estimating potential evapotranspiration. Journal of the Hydraulics Division 87, 107–120. Publisher: American Society of Civil Engineers.

Jemeljanova, M., Collenteur, R.A., 2022. Modeling hydraulic heads with impulse response functions in different environmental settings (dataset and code supplement). doi:10.5281/zenodo.7403401.

Kavetski, D., Fenicia, F., Clark, M.P., 2011. Impact of temporal data resolution on parameter inference and model identification in conceptual hydrological modeling: Insights from an experimental catchment. Water Resources Research 47. URL: https://doi.org/10.1029/2010WR009525, doi:10.1029/2010WR009525. publisher: John Wiley & Sons, Ltd.

Kavetski, D., Kuczera, G., 2007. Model smoothing strategies to remove microscale discontinuities and spurious secondary optima in objective functions in hydrological calibration. Water Resources Research 43. URL: https://doi.org/10.1029/2006WR005195, doi:10.1029/2006WR005195. publisher: John Wiley & Sons, Ltd.

Kling, H., Fuchs, M., Paulin, M., 2012. Runoff conditions in the upper Danube basin under an ensemble of climate change scenarios. Journal of Hydrology 424-425, 264 – 277. URL: http://www.sciencedirect.com/science/article/pii/S0022169412000431, doi:https://doi.org/10.1016/j.jhydrol.2012.01.011.

Kobel, R., 2009. Zürich HB, Durchmesserlinie Altstetten – Zürich HB – Oerlikon, in: MITTEILUNGEN der Schweizerischen Gesellschaft für Boden- und Felsmechanik, Swiss Geotechnics Association, Zürich. p. 104.

Kong, F., Song, J., Crosbie, R.S., Barron, O., Schafer, D., Pigois, J.P., 2021. Groundwater Hydrograph Decomposition With the HydroSight Model. Frontiers in Environmental Science 9, 306. URL: https://www.

frontiersin.org/article/10.3389/fenvs.2021.736400, doi:10.3389/fenvs.2021.736400.

Liu, Z., Wang, Y., Xu, Z., Duan, Q., 2019. Conceptual Hydrological Models, in: Duan, Q., Pappenberger, F., Wood, A., Cloke, H.L., Schaake, J.C. (Eds.), Handbook of Hydrometeorological Ensemble Forecasting. Springer Berlin Heidelberg, Berlin, Heidelberg, pp. 389–411. URL: https://doi.org/10.1007/978-3-642-39925-1_22, doi:10.1007/978-3-642-39925-1_22.

Lundberg, A., Ala-Aho, P., Eklo, O., Klöve, B., Kværner, J., Stumpp, C., 2016. Snow and frost: implications for spatiotemporal infiltration patterns – a review. Hydrological Processes 30, 1230–1250. URL: https://onlinelibrary.wiley.com/doi/abs/10.1002/hyp.10703, doi:https://doi.org/10.1002/hyp.10703. _eprint: https://onlinelibrary.wiley.com/doi/pdf/10.1002/hyp.10703.

Mackay, J.D., Jackson, C.R., Wang, L., 2014. A lumped conceptual model to simulate groundwater level time-series. Environmental Modelling and Software 61, 229–245. URL: http://www.sciencedirect.com/science/article/pii/S1364815214001674, doi:https://doi.org/10.1016/j.envsoft.2014.06.003.

Manzione, R.L., Soldera, B.C., Wendland, E.C., 2017. Groundwater system response at sites with different agricultural land uses: case of the Guarani Aquifer outcrop area, Brotas/SP-Brazil. Hydrological Sciences Journal 62, 28–35. URL: https://doi.org/10.1080/02626667.2016.1154148, doi:10.1080/02626667.2016.1154148.

Marchant, B., Mackay, J., Bloomfield, J., 2016. Quantifying uncertainty in predictions of groundwater levels using formal likelihood methods. Journal of Hydrology 540, 699 – 711. URL: http://www.sciencedirect.com/science/article/pii/S0022169416303651, doi:https://doi.org/10.1016/j.jhydrol.2016.06.014.

Marshall, L., Nott, D., Sharma, A., 2005. Hydrological model selection: A Bayesian alternative. Water Resources Research 41. URL: https://doi.org/10.1029/2004WR003719, doi:10.1029/2004WR003719. publisher: John Wiley & Sons, Ltd.

Meeks, J., Moeck, C., Brunner, P., Hunkeler, D., 2017. Infiltration under snow cover: Modeling approaches and predictive uncertainty. Journal of Hydrology 546, 16–27. URL: https://www.sciencedirect.com/science/article/pii/S0022169416308290, doi:10.1016/j.jhydrol.2016.12.042.

MeteoSwiss, 2022. RhiresD and TabsD gridded precipitation and temperature data sets. URL: https://www.meteoswiss.admin.ch/home/climate/swiss-climate-in-detail/raeumliche-klimaanalysen.html?query=TabsD.

Moeck, C., von Freyberg, J., Schirmer, M., 2018. Groundwater recharge predictions in contrasted climate: The effect of model complexity and calibration period on recharge rates. Environmental Modelling & Software 103, 74–89. URL: https://www.sciencedirect.com/science/article/pii/S1364815216309458, doi:10.1016/j.envsoft.2018.02.005.

Peterson, T.J., Western, A.W., 2014. Nonlinear time-series modeling of unconfined groundwater head. Water Resources Research 50, 8330–8355. URL: http://onlinelibrary.wiley.com/doi/10.1002/2013WR014800/abstract, doi:10.1002/2013WR014800.

Schürch, M., Vuataz, F.D., 2000. Groundwater components in the alluvial aquifer of the alpine Rhone River valley, Bois de Finges area, Wallis Canton, Switzerland. Hydrogeology Journal 8, 549–563. URL: https://doi.org/10.1007/s100400000094, doi:10.1007/s100400000094.

Shapoori, V., Peterson, T.J., Western, A.W., Costelloe, J.F., 2015a. Decomposing groundwater head variations into meteorological and pumping components: a synthetic study. Hydrogeology Journal 23, 1431–1448. URL: https://doi.org/10.1007/s10040-015-1269-7, doi:10.1007/s10040-015-1269-7.

Shapoori, V., Peterson, T.J., Western, A.W., Costelloe, J.F., 2015b. Top-down groundwater hydrograph time-series modeling for climate-pumping decomposition. Hydrogeology Journal 23, 819–836. URL: http://link.springer.com/article/10.1007/s10040-014-1223-0, doi:10.1007/s10040-014-1223-0.

Van der Spek, J.E., Bakker, M., 2017. The influence of the length of the calibration period and observation frequency on predictive uncertainty in time series modeling of groundwater dynamics. Water Resources Research 53, 2294–2311. URL: https://agupubs.onlinelibrary.wiley.com/doi/abs/10.1002/2016WR019704, doi:10.1002/2016WR019704.

Stoffer, D.S., Toloi, C.M.C., 1992. A note on the Ljung—Box—Pierce portmanteau statistic with missing data. Statistics & probability letters 13, 391–396. Publisher: Elsevier.

Taylor, R.G., Scanlon, B., Döll, P., Rodell, M., van Beek, R., Wada, Y., Longuevergne, L., Leblanc, M., Famiglietti, J.S., Edmunds, M., Konikow, L., Green, T.R., Chen, J., Taniguchi, M., Bierkens, M.F.P., MacDonald, A., Fan, Y., Maxwell, R.M., Yechieli, Y., Gurdak, J.J., Allen, D.M., Shamsudduha, M., Hiscock, K., Yeh, P.J.F., Holman, I., Treidel, H., 2013. Ground water and climate change. Nature Climate Change 3, 322–329. URL: https://www.nature.com/articles/nclimate1744, doi:10.1038/nclimate1744.

Vremec, M., Collenteur, R.A., 2022. PyEt: A Python package for estimating evaporation. URL: https://doi.org/10.5281/zenodo.5896800, doi:10.5281/zenodo.5896800.

Zaadnoordijk, W.J., Bus, S.A.R., Lourens, A., Berendrecht, W.L., 2019. Automated Time Series Modeling for Piezometers in the National Database of the Netherlands. Groundwater 57, 834–843. URL: https://ngwa.onlinelibrary.wiley.com/doi/abs/10.1111/gwat.12819, doi:10.1111/gwat.12819.